Journal of Applied Physics

1 GeV proton damage in β-Ga_2O_3

Cite as: J. Appl. Phys. **130**, 185701 (2021); https://doi.org/10.1063/5.0068306
Submitted: 24 August 2021 • Accepted: 21 October 2021 • Published Online: 08 November 2021

A. Y. Polyakov, I. V. Shchemerov, A. A. Vasilev, et al.

AIP Publishing

Journal of Applied Physics ARTICLE scitation.org/journal/jap

1 GeV proton damage in β-Ga_2O_3

Cite as: J. Appl. Phys. **130**, 185701 (2021); doi: 10.1063/5.0068306
Submitted: 24 August 2021 · Accepted: 21 October 2021 ·
Published Online: 8 November 2021

A. Y. Polyakov,[1] I. V. Shchemerov,[1] A. A. Vasilev,[1] A. I. Kochkova,[1] N. B. Smirnov,[1] A. V. Chernykh,[1] E. B. Yakimov,[1,2] P. B. Lagov,[1,3] Yu. S. Pavlov,[3] E. M. Ivanov,[4] O. G. Gorbatkova,[4] A. S. Drenin,[5] M. E. Letovaltseva,[6] Minghan Xian,[7] Fan Ren,[7] Jihyun Kim,[8] and S. J. Pearton[9,a)]

AFFILIATIONS

[1]National University of Science and Technology MISiS (NUST MISiS), Moscow 119049, Russia
[2]Institute of Microelectronics Technology RAS, Chernogolovka 142432, Russia
[3]Laboratory of Radiation Technologies, Frumkin Institute of Physical Chemistry and Electrochemistry Russian Academy of Sciences (IPCE RAS), 31 Leninsky prospect, build. 4, Moscow 119071, Russia
[4]National Research Centre "Kurchatov Institute," Petersburg Nuclear Physics Institute (PNPI), 1 Orlova roshcha, Gatchina 188300, Russian Federation
[5]LLC Research and Development Enterprise "Collider," Moscow 119017, Russia
[6]Russian Technological University MIREA (RTU MIREA), 78 Vernadsky Avenue, Moscow 119454, Russia
[7]Department of Chemical Engineering, University of Florida, Gainesville, Florida 32611, USA
[8]Department of Chemical and Biological Engineering, College of Engineering, Korea University, Anam-dong 5-1, Sungbuk-gu, Seoul 02841, South Korea
[9]Department of Material Science and Engineering, University of Florida, Gainesville, Florida 32611, USA

Note: This paper is part of the Special Topic on Wide Bandgap Semiconductor Materials and Devices.
[a)]**Author to whom correspondence should be addressed:** spear@mse.ufl.edu

ABSTRACT

The changes of electrical properties and deep trap spectra induced in n-type β-Ga_2O_3 by 1 GeV protons with a fluence of 4×10^{13} cm^{-2} were studied. The carrier removal rates were ~100 cm^{-1} at this energy. For comparison, for 20 MeV proton irradiation at comparable fluences ($5–10 \times 10^{14}$ cm^{-2}), the removal rate was ~400 cm^{-1} for donor concentrations of 3×10^{16} cm^{-3} and ~100 cm^{-1} for concentrations of $<10^{16}$ cm^{-3}. These removal rates were in stark contrast with modeling results that predicted the introduction rates of vacancies to be two orders of magnitude higher for 20 MeV protons. Measurements of deep electron and hole traps densities by deep level transient spectroscopy with electrical or optical injection (DLTS or ODLTS), and capacitance–voltage profiling under monochromatic light illumination showed that the 1 GeV proton irradiation resulted in the introduction of deep donors E2*(E_c-0.75 eV) and E3 (E_c-1 eV) and deep acceptors with optical ionization threshold near 2.3 eV producing a feature near 250 K in ODLTS and 3.1 eV with related ODLTS feature near 450 K. The total concentration of all deep traps was much lower than that necessary to explain the observed decrease in net donor density upon irradiation. The donor densities showed a nonuniform distribution in proton irradiated films with the concentration greatly decreased toward the surface. Possible reasons for the observed performance are discussed.

I. INTRODUCTION

Recent years have seen an impressive progress in the growth of high crystalline quality β-Ga_2O_3 bulk crystals and epilayers and in the fabrication of high-power devices based on this material. The interest is stimulated due to the very high critical electric field near 6–8 MV/cm, much higher than the more established wide-bandgap materials GaN or SiC.[1–4] An additional attractive feature of Ga_2O_3 is that experiments with protons, neutrons, electrons, and γ-irradiation show that it has a high radiation tolerance on par with that of GaN or SiC.[5,6] This is an important consideration as wide-bandgap power devices are increasingly finding their way into electronic systems operating in space and avionics where they supplant Si-based devices due to better performance and

lighter weight.[7] However, so far the bulk of radiation experiments in Ga_2O_3 structures was done with moderate energies, such as protons with energies 1–20 MeV, reactor neutrons, and 18 MeV alpha-particles.[8–12] There is also interest in the response of Ga_2O_3 to the very high energy (GeV) protons encountered in galactic cosmic ray fluxes in deep space applications.[5–7]

Presently, little is known of the response of Ga_2O_3 to such irradiation. In this article, we report the results of electrical and deep trap studies performed on β-Ga_2O_3 epi structures subjected to irradiation with 1 GeV protons and also compare the results to those with 20 MeV protons.

II. EXPERIMENTAL

The samples were β-polytype Si doped n-Ga_2O_3(Si) films grown by Halide Vapor Phase Epitaxy (HVPE) on Sn doped n-Ga_2O_3(Sn) substrates cut from bulk single crystals grown by Edge-defined Film-fed Growth (EFG). The structures were acquired from Tamura/Novel Crystals Co. (Japan). The net electron concentration of the films was approximately 10^{15}–10^{16} cm^{-3}, and the thickness was 7–10 μm. The net donor density of the substrates was 3×10^{18} cm^{-3}. The orientation of the structures was (001). Seven samples were studied. Samples S1, S2, S3, S4, and S5 were epi structures for which the back Ohmic contacts were prepared by Ti/Au (20 nm/80 nm) e-beam evaporation with subsequent rapid thermal annealing at 500 °C for 30 s in nitrogen. Ni Schottky diodes on the front surface were made by e-beam evaporation of Ni (20 nm) through a shadow mask. The diameter of the circular diodes was 1 mm.

Table I summarizes the samples and proton irradiation conditions. Sample S1 had a starting net donor concentration established by room temperature capacitance–voltage profiling of 3×10^{16} cm^{-3}. This sample was subjected to irradiation with 20 MeV protons with fluences of 5×10^{13} and 10^{14} cm^{-2} (designated as S1-5×10^{13} and S1-10^{14}). Sample S2 had a starting concentration of 10^{16} cm^{-3} and was irradiated with a fluence of 20 MeV protons of 10^{14} cm^{-2} (sample S2-10^{14}). Sample 3 had a starting concentration of 3×10^{15} cm^{-3} and was irradiated with a fluence of 4×10^{13} cm^{-2} of 1 GeV protons (sample S3-4×10^{13} GeV). Sample S4 had a starting concentration of 1.2×10^{16} cm^{-3} and was irradiated with 20 MeV protons with a fluence of 10^{14} cm^{-2} (sample S4-10^{14}). Sample S5 had a concentration of 10^{16} cm^{-3} and was subjected to irradiation with a fluence of 4×10^{13} cm^{-2} of 1 GeV protons (sample S5-4×10^{13} GeV).

Samples 6 and 7 were processed into rectifier structures with backside Ti/Au (20 nm/80 nm) deposited by e-beam evaporation and rapid thermal annealing at 550 °C for 30 s in nitrogen. The Schottky diodes on the front surface were prepared by first dc sputtering of 20 nm W layer and then e-beam evaporation of 340 nm Au. Then, photolithographic patterning was done to produce 400 μm square diodes and circular diodes with diameters 200 and 150 μm. No dielectric layers surface passivation or plate electrodes were used. The samples were then mounted on a transistor header and wire-bonded for subsequent measurements, as illustrated in Fig. 1S in the supplementary material. Sample S6 was irradiated with 20 MeV protons with a fluence of 10^{14} cm^{-2} (sample S6-10^{14}). Sample S7 was irradiated with a fluence of 4×10^{13} cm^{-2} of 1 GeV protons (sample S7-4×10^{13} GeV).

Characterization before and after proton irradiation included capacitance–voltage (C–V) profiling and light C-V (LCV) profiling spectra measurements[13,14] with excitation from high-power (optical power 250 mW/cm^2) light emitting diodes (LEDs) with peak photon energies ranging from 1.35 to 3.4 eV or with UV LEDs emitting at 259.4 nm (photon energy 4.8 eV, optical power 1.2 mW/cm^2). Deep electron trap spectra were obtained from deep level transient spectroscopy (DLTS)[15,16] measurements in the temperature range 80–500 K using a gas-flow nitrogen cryostat

TABLE I. Changes in net donor density N_d and in carrier removal rate dN_d/dF for samples irradiated with 1 GeV or 20 MeV protons with fluences F; for samples S4, S4-10^{14}, S5, and S5-4×10^{13} GeV also shown are the changes in concentrations of the deep acceptors with optical thresholds 2.3 and 3.1 eV caused by 1 GeV and 20 MeV proton irradiations.

Sample #	Type of proton treatment	N_d (cm^{-3})	dN_d/dF (cm^{-1})	2.3 eV concentration (cm^{-3})	3.1 eV concentration (cm^{-3})
S1	None	3×10^{16}	–		
S1-5×10^{13}	20 MeV protons, F = 5×10^{13} cm^{-2}	10^{16}	400		
S1-10^{14}	20 MeV protons, F = 10^{14} ($5 \times 10^{13} + 5 \times 10^{13}$) cm^{-2}	10^{15}	200		
S2	None	10^{16}	–		
S2-10^{14}	20 MeV protons, F = 10^{14} cm^{-2}	3×10^{14}	100		
S3	None	2×10^{15}	–		
S3-4×10^{13}	1 GeV protons, F = 4×10^{13} cm^{-2}	10^{14}	72.5		
S4	None	1.3×10^{16}	–	2×10^{14}	–
S4-10^{14}	20 MeV protons, F = 10^{14} cm^{-2}	3×10^{13}	120	1.2×10^{15}	4×10^{14}
S5	None	10^{16}	–	3×10^{14}	–
S5-4×10^{13} GeV	1 GeV protons, F = 4×10^{13} cm^{-2}	4×10^{15}	137.5	7.5×10^{14}	2.8×10^{14}
S6	None	1.3×10^{16}	–		
S6-10^{14}	20 MeV protons, F = 10^{14} cm^{-2}	4×10^{15}	90		
S7	None	9×10^{15}	–		
S7-4×10^{13} GeV	1 GeV protons, F = 4×10^{13} cm^{-2}	6×10^{15}	75		

(Cryotrade Company, Russia). Hole trap spectra were measured by DLTS measurements with optical excitation (ODLTS)[17,18] with above-bandgap (4.8 eV LED) LED excitation. A detailed description of experimental setups can be found in our earlier papers.[11,12,16,19]

The diffusion lengths of nonequilibrium charge carriers were calculated from the electron beam energy dependence of the normalized electron beam induced current (EBIC) of a scanning electron microscope.[20,21]

20 MeV proton irradiations were performed on linear accelerator I-2 at the Center of Collective Use "Kamiks" of ITEP (Russia) that has been used successfully to control the switching characteristics of Si power devices.[22,23] The fluences used were 5×10^{13} or 10^{14} cm^{-2} with a flux of 10^{11} cm^{-2} s^{-1}. High energy 1 GeV proton irradiation was performed on the synchrocyclotron SC-1000[24–26] at the PNPI accelerator department (Russia). The total fluence was 4×10^{13} cm^{-2} at a flux of 3×10^{10} cm^{-2} s^{-1}.

The damage profiles were obtained from the Stopping-and-Range-of-Ions-in-Matter (SRIM) code,[27,28] which calculates the screened Coulombic collision rate between an incoming ion and the atoms in the target. An ion traversing Ga_2O_3 undergoes collisions with the target atoms. The total energy loss per unit distance is determined by electronic stopping and nuclear stopping. In the former, ion energy is lost by excitation and ionization of atoms, dissipating as heat, and not creating atomic displacements. Nuclear stopping occurs through elastic collisions of ions with nuclei or atoms, with part of the kinetic energy of the incoming ion transferred to displace nuclei, creating deep-level compensating defects.

III. RESULTS AND DISCUSSION

C-V characteristics of the Ni Schottky diodes before and after irradiation causing relatively low changes in net donor density were in good agreement with the previously published data. The Schottky barrier heights obtained from the built-in voltage of the $1/C^2$ vs V plots were close to 1 eV, and the plots were reasonably linear [e.g., Fig. 2S(a) in the supplementary material depicts data for S4, S5, and S5-4×10^{13} GeV]. These samples showed ideality factors close to 1 and low reverse leakage currents of the Schottky diodes that allowed DLTS spectra measurements at high reverse voltages even at 500 K. For the samples with refractive W Schottky diodes, the Schottky barrier heights were 0.6 eV [Fig. 2S(b) in the supplementary material shows data for S7 and S7-4e13 GeV]. The lower Schottky barrier height resulted in higher reverse leakage at 500 K and restricted the reverse biases in DLTS to voltages below ~2 V, although, at 300 K, the reverse current in I-V characteristics was still low.

However, in general, proton irradiated samples showed the nonuniform distribution of net donor densities that often demonstrated a decrease in concentration toward the surface of the films so that concentration profiles had to be built by differentiating the $1/C^2$ vs voltage characteristics by voltage.[29] Panels (a) of Figs. 1–3 present such room temperature concentration profiles for all samples, while panels (b) of these figures depict the changes in concentration close to the surface and give the estimates of the carrier removal rates induced by irradiation for particular fluences and proton energies. The data of Figs. 1–3 are summarized in Table I that also specifies the starting concentrations of the samples and the energy and fluence of the protons used.

Several points are clear from Figs. 1–3. First, as the proton fluences increase, the net donor concentrations tend to become more nonuniform and more depleted toward the surface. For example, in samples S1-10^{14}, S2-10^{14}, and S4-10^{14} irradiated with 10^{14} cm^{-2} of 20 MeV protons, and sample S3-4×10^{13} GeV irradiated with 4×10^{13} cm^{-2} 1 GeV protons, the concentrations strongly decrease toward the surface and the sample S4-10^{14} is depleted almost down to the interface with the n^+ substrate (the thickness of this film is 7 μm). SRIM modeling predicts a uniform distribution of primary vacancies across the thickness of the film [the results for calculated vacancies concentration vs thickness for 20 MeV and 1 GeV are shown in Figs. 4(a) and 4(b) together with the distribution of hydrogen ions]. This suggests a marked redistribution of primary defects in the irradiated samples. Since the concentration of primary hydrogen ions within the n-Ga_2O_3 films of ~10 μm thickness is negligible (see Fig. 4) and since it is known that hydrogen out-diffusion in proton-irradiated β-Ga_2O_3 does not start for

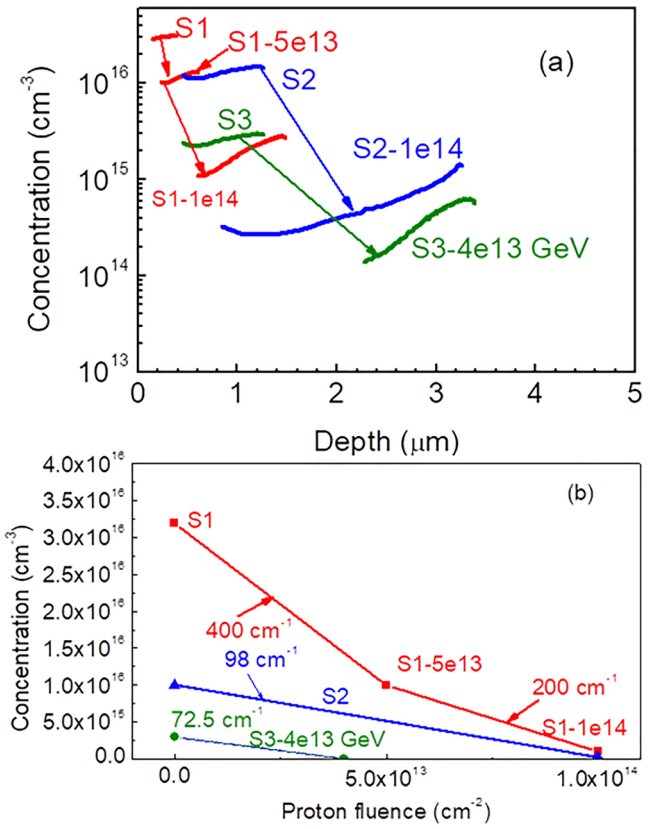

FIG. 1. (a) Concentration profiles measured before and after irradiation with 20 MeV protons for samples S1, S1-5 × 10^{13}, S1-10^{14}, S2, S2-10^{14} and sample S3 before irradiation with 1 GeV protons and sample S3-4 × 10^{13} GeV after irradiation with a fluence of 4×10^{13} cm^{-2} 1 GeV protons; (b) concentration changes near the surface and estimated carrier removal rates.

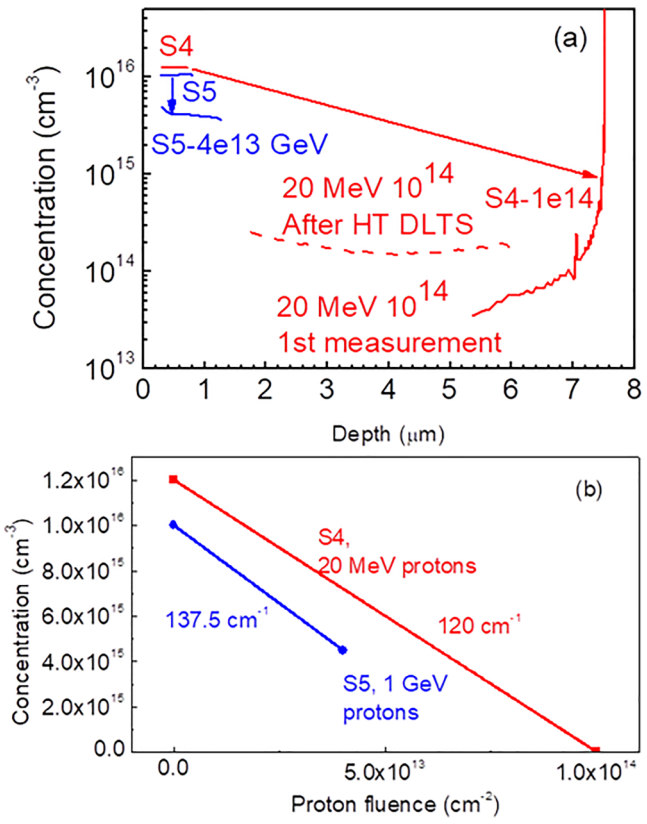

FIG. 2. (a) Concentration profiles measured before and after irradiation with 20 MeV protons for samples S4, S1-1e14, and sample S5 before irradiation with 1 GeV protons and sample S3-4e13 GeV after irradiation with a fluence of 4×10^{13} cm^{-2} 1 GeV protons; (b) estimated concentration changes and carrier removal rates.

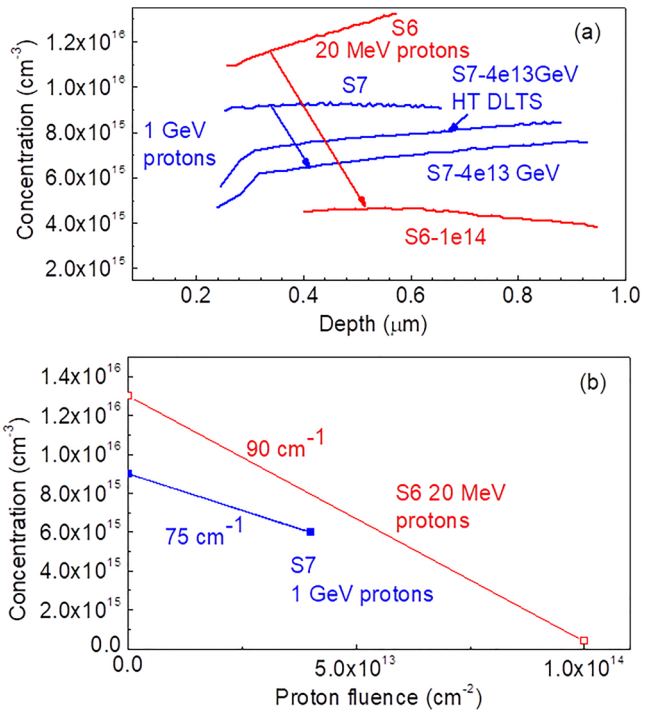

FIG. 3. (a) Concentration profiles measured before and after irradiation with 20 MeV protons for samples S6, S6-1e14, and sample S7 before irradiation with 1 GeV protons and sample S7-4×10^{13} GeV after irradiation with a fluence of 4×10^{13} cm^{-2} 1 GeV protons; (b) estimated concentration changes and carrier removal rates.

temperatures <~500 °C,[30] it appears that the moving species should be native point defects. Moreover, in our DLTS measurements, we observed that the charge redistribution occurs already during DLTS spectra collection at high temperatures [see Figs. 2(a) and 3(a)].

Some preliminary experiments carried out by us show that measurable changes in observed concentration profiles start for temperatures higher than 400 K and are accelerated when reverse bias is applied (see Fig. 3S in the supplementary material; the figure was obtained for sample S1-10^{14} after DLTS measurement up to 400 K and subsequent annealing between 320 and 420 K for 20 min). Second, the removal rates for protons with energies 20 MeV and 1 GeV are not different, whereas modeling predicts more than two orders of magnitude difference in the concentration of primary native defects (Fig. 4). Third, the removal rates tend to decrease with a decrease in the starting net donor concentration. These features require a better understanding. The results suggest that compensating (or passivating) native defects tend to gravitate toward the surface of irradiated films, and the degree of compensation or passivation becomes higher for higher net donor densities. The effect of this compensation/passivation is partially annealed at temperatures as low as ~400 K.

Somewhat similar behavior has been previously reported for β-Ga_2O_3 irradiated with (0.6–2) MeV protons.[9,31] This compensation has been attributed to the formation of split Ga vacancy defects V^i_{Ga} (Refs. 9 and 31–34) and their partial passivation with hydrogen. These split vacancies V^i_{Ga} are believed to give rise to a dominant photocapacitance band with an optical threshold near 2.3 eV and a rather high (~0.5 eV) barrier for the capture of electrons, causing a prominent persistent photocapacitance that cannot be quenched by the application of the forward bias.[13,14,32] Such centers are routinely observed in our β-Ga_2O_3 films alongside other deep acceptor defects with an optical threshold near 3.1 eV whose origin is not clear, but has been tentatively attributed to V_{Ga} acceptors[8,11,12] or V_{Ga}–V_O divacancies.[32] We measured their concentration before and after proton irradiation for sample S4 irradiated with 20 MeV protons and sample S5 irradiated with 1 GeV protons. These concentrations are presented in Table I for samples S4, S4-10^{14}, S5, and S5-4×10^{13} GeV. Compensating acceptors of that kind are indeed introduced by 20 MeV and 1 GeV protons at similar rates, but their densities are too low to account for the observed carrier removal rates in irradiated samples.

Other deep level spectra studies using DLTS and ODLTS also have not revealed the proton-induced formation of deep acceptors

that could be responsible for the observed carrier removal rates. DLTS measurements for the starting samples were dominated by the common features due to the well-known electron traps near E_c-0.5 eV (E1 centers[5,9]), E_c-0.8 eV (E2), a low temperature shoulder near 270 K that could be distinguished by fitting the individual capacitance relaxation curves or by Laplace DLTS analysis[11,19] as belonging to the E_c-0.7 eV centers known in the literature as the E2* traps,[9] and, at the highest measurement temperatures, traps near E_c-1 eV known in the literature as the E3 traps[5,9] [Figs. 5(a)–5(c)].

The E2 defects have been reliably attributed to substitutional Fe acceptors on the Ga sites[35] on the strength of a clear correlation between their density and the density of Fe determined by secondary ion mass spectrometry,[35] the behavior of the DLTS peak emission rate on electric field strength,[19,36] comparison with the features of the dominant compensating center in Fe-doped semi-insulating β-Ga_2O_3,[37,38] and finally on theoretical calculations.[35] The E3 traps are known to be deep donors, judging by the electric field dependence of the DLTS emission rate,[19,36] as also is the case with the E2* center.[39] The E3 traps have been attributed to Ir-related donors,[36] but have also been associated with native defects introduced by irradiation.[5] The E2* traps are known to be native point defects. Their density increases under irradiation with high energy particles,[5] and they could be responsible for lifetime degradation in β-Ga_2O_3.[8,12,31,39] Recently, some arguments have been advanced in favor of these centers being related to gallium vacancies–oxygen vacancy V_{Ga}–V_O complexes (divacancies).[31,39]

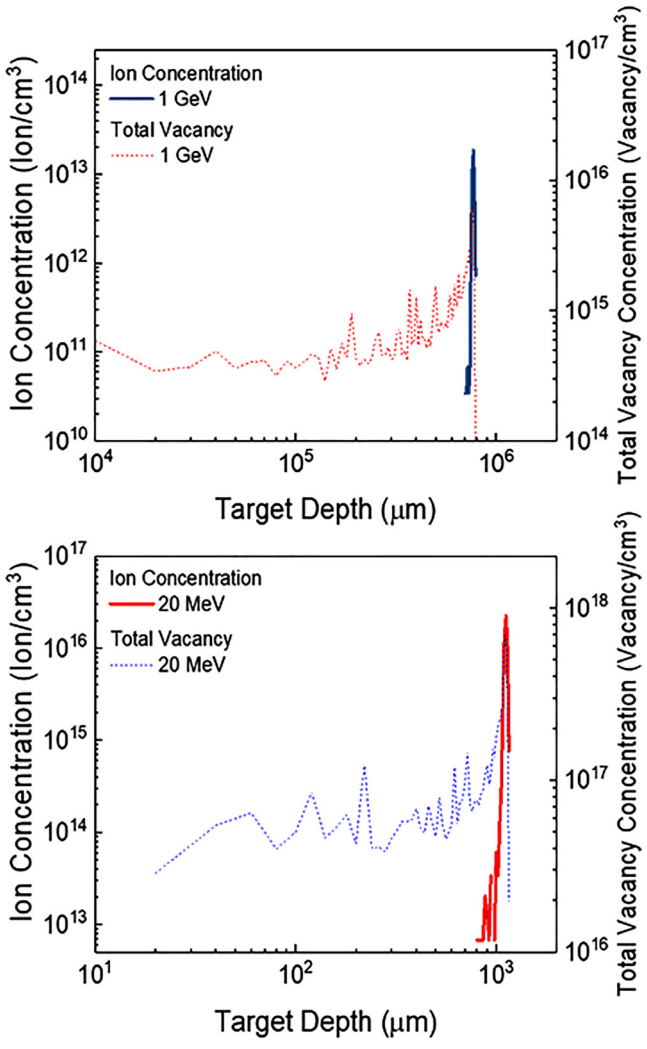

FIG. 4. (a) Hydrogen ion concentrations and total vacancy concentration profiles calculated by SRIM for the 20 MeV proton fluence of 10^{14} cm^{-2} (mean introduction rate of vacancies in the top 10 μm of 500 cm^{-1}); (b) the same for 1 GeV protons with a fluence of 4×10^{13} cm^{-2} (mean introduction rate ~10 cm^{-1}).

Proton irradiation with high fluences led in most cases to a strong compensation and a marked nonuniformity of net donor densities not conducive to accurate determination of deep trap densities (Figs. 1–3). However, in the cases where the donor densities changes were not so strong, DLTS was reliable. Figures 5(a)–5(c) show the evolution of DLTS spectra after proton irradiation. The y axes in the figures are taken to be the product of the DLTS signal $\Delta C/C$, 2 N_d, and F^{-1}, $2N_d \times \Delta C/C \times F^{-1}$. Here, ΔC is the difference in transient capacitances measured at time windows t1 and t2, $\Delta C = C(t1) - C(t2)$, C is the stationary capacitance at the temperature of measurements, and F^{-1} is the DLTS spectrometer function converting the ΔC signal into the full capacitance relaxation amplitude.[15]

For the temperatures corresponding to the peaks in DLTS spectra, the peak amplitudes in such coordinates give the concentrations of respective traps without the so-called λ-correction that accounts for the fact that the deep traps are not recharged in the entire space charge region by the bias pulse in DLTS.[15] The data of Fig. 5 show that when the deep electron trap concentrations can be reliably determined in DLTS [for sample S1 irradiated with 5×10^{13} and 10^{14} cm^{-2} 20 MeV protons (Fig. 5(a)), for sample S5 irradiated with 4×10^{13} cm^{-2} 1 GeV protons (Fig. 5(b)), for sample S6 irradiated with 10^{14} cm^{-2} 20 MeV protons and sample S7 irradiated with 4×10^{13} cm^{-2} 1 GeV protons (Fig. 5(c))], proton irradiation introduces new electron traps with level near E_c-(0.25–0.3) eV (E8),[5] slightly increases the concentration of the E_c-0.5 eV (E1) trap, increases the density of the E2* trap, does not change the concentration of the E2 trap due to Fe acceptors, and strongly increases the concentration of the E3 centers. For the irradiated S7 sample, we also observe the introduction of a prominent trap near E_c-1.3 eV (E4 trap).[9,11,12]

These latter traps are also prominent in the spectra of the S3 sample after irradiation with 4×10^{13} cm^{-2} 1 GeV protons although the peak amplitudes are not easily converted into concentrations because of the strong nonuniformity of net donor concentration (see Fig. 4S in the supplementary material). The general conclusion is that, even with the λ-correction to the deep electron trap concentrations taken into account, the centers observed after proton irradiation cannot explain the observed carrier removal rates or the nonuniformity of concentration profiles in irradiated samples.

DLTS spectra measured with optical excitation with 259-nm LEDs are shown for the S1 sample after irradiation with 20 MeV protons in Fig. 6(a), and the spectra for the S4 sample irradiated

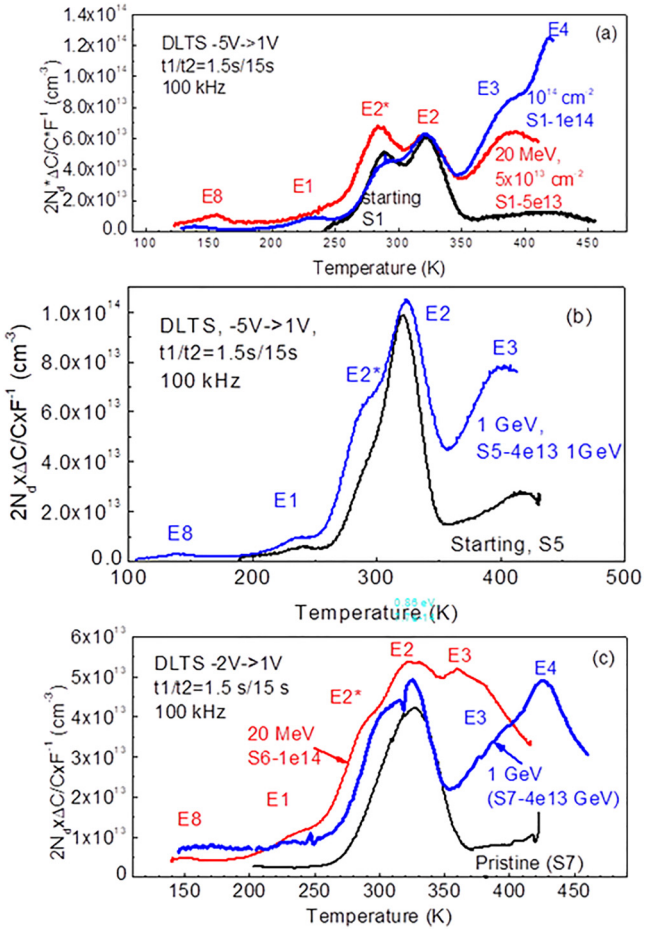

FIG. 5. (a) DLTS spectra changes induced in sample S1 by 20 MeV protons irradiation with fluences 5×10^{13} and $10^{14}\,cm^{-2}$; (b) the same for sample S5 irradiated with $4 \times 10^{13}\,cm^{-2}$ 1 GeV protons; (c) DLTS spectra changes induced in samples S6 and S7 by irradiations with $10^{14}\,cm^{-2}$ 20 MeV protons and $4 \times 10^{13}\,cm^{-2}$ 1 GeV protons (the starting spectrum is shown only for sample S7, and for sample S6, the spectrum was the same, with the main feature due to the E2 Fe-related trap); the conditions of DLTS spectra acquisition are shown in the figures; for the S6 and S7 samples in (c), the reverse bias was −2 V instead of −5 V because of the lower Schottky barrier height of W compared to Ni and consequently higher leakage at high temperatures.

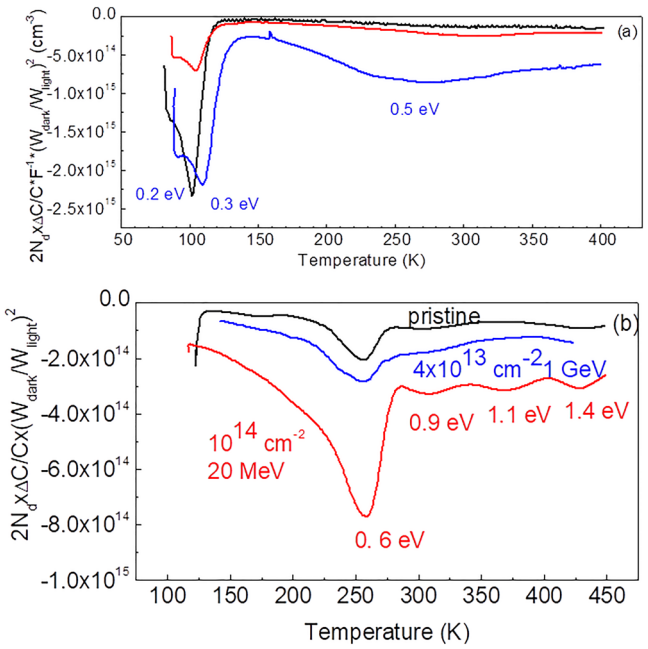

FIG. 6. (a) ODLTS spectra measured for the S1 sample before proton irradiation (black line) and after 20 MeV proton irradiation with fluences $5 \times 10^{13}\,cm^{-2}$ (red line) and $10^{14}\,cm^{-2}$ (blue line); (b) ODLTS spectra measured for sample S4 before and after irradiation with 10^{14} cm^{-2} 20 MeV protons (red line) and for sample S5 after irradiation with 4×10^{13} cm^{-2} 1 GeV protons (blue line) (the starting spectrum for sample S5 is very similar to S4); measurements conditions: reverse bias −1 V, excitation pulse by 259 nm wavelength LED (5-s-long, optical power 1.2 mW/cm^2), time windows 1.75 s/17.5 s.

with $10^{14}\,cm^{-2}$ 20 MeV protons and S5 sample irradiated with $4 \times 10^{13}\,cm^{-2}$ 1 GeV protons are shown in Fig. 6(b) (the spectra in samples S4 and S5 before irradiation were similar, and only the spectrum for sample S5 is shown). The y axis in the figures is, as with DLTS spectra mentioned earlier, taken as $2N_d \times \Delta C/C \times F^{-1}$, but it is additionally multiplied by the ratio of squared space charge region (SCR) widths in the dark and under illumination $(W_{dark}/W_{light})^2$. This reflects the fact that, for deep acceptors with levels below the Fermi level, these acceptors are only recharged in the SCR region where the light is effectively absorbed.[17] As with DLTS, in such coordinates, the amplitudes of ODLTS peaks approximately correspond to the density of deep acceptors.[17] The width of the SCR down to which the light affects the space charge distribution was obtained by C-V profiling under illumination and was found to be ∼0.5 μm. All ODLTS measurements were done with applied bias −1 V and the corresponding values of W_{dark}, as well as the net donor densities were taken from the C-V profiling.

As shown in Fig. 6(a), the spectra consist of a prominent doublet feature near 100 K with activation energies 0.2 and 0.3 eV. This doublet was attributed[18,40] to transitions from the self-trapped polaronic hole (STH) states located near the oxygen sites O1 and O2 into the proper valence hole states. Such STH states are predicted by theory, and their existence is a hindrance to hole conduction in Ga_2O_3.[9,33,34] The peak near 250 K has the activation energy of 0.5 eV. No acceptor states with levels so close to the valence band have been predicted by theory[41] or detected in experiments.[1–3] The value of the activation energy is close to the barrier height for changing the charge state of the split Ga vacancies V^i_{Ga} from −2 to −1 as determined by deep level optical spectroscopy (DLOS).[13,14] This transition persistently increases the charge and the measured capacitance in the SCR after illumination, so the capacitance transient after the light is switched off will be hole-trap-like (the capacitance decreases with time after the light pulse and the amplitude of the peak is the measure of the concentration of the centers recharged by light).

For sample S3 irradiated with 4×10^{13} cm^{-2} 1 GeV protons, we observed in ODLTS spectra additional peaks with activation energies 1.1 and 1.4 eV (see Fig. 5S in the supplementary material). ODLTS spectra for samples S4 irradiated with 10^{14} cm^{-2} 20 MeV protons and S5 irradiated with 4×10^{13} cm^{-2} 1 GeV protons are shown in Fig. 6(b) (for technical reasons, the lowest temperature part of the spectra with self-trapped holes peaks was not measured for this set). In addition to the 0.5 eV peak, we also observed at high temperatures, peaks with activation energies 0.9, 1.1, and 1.4 eV. The amplitudes of the 0.5 eV peak are close to the density of deep acceptor traps with the optical threshold near 2.3 eV in LCV spectra, while the concentration of the 1.4 eV center in ODLTS is close to the density of the acceptor traps with optical ionization threshold 3.1 eV in LCV (see Table I), which suggests that in both measurements one is dealing with similar centers (see Table I).

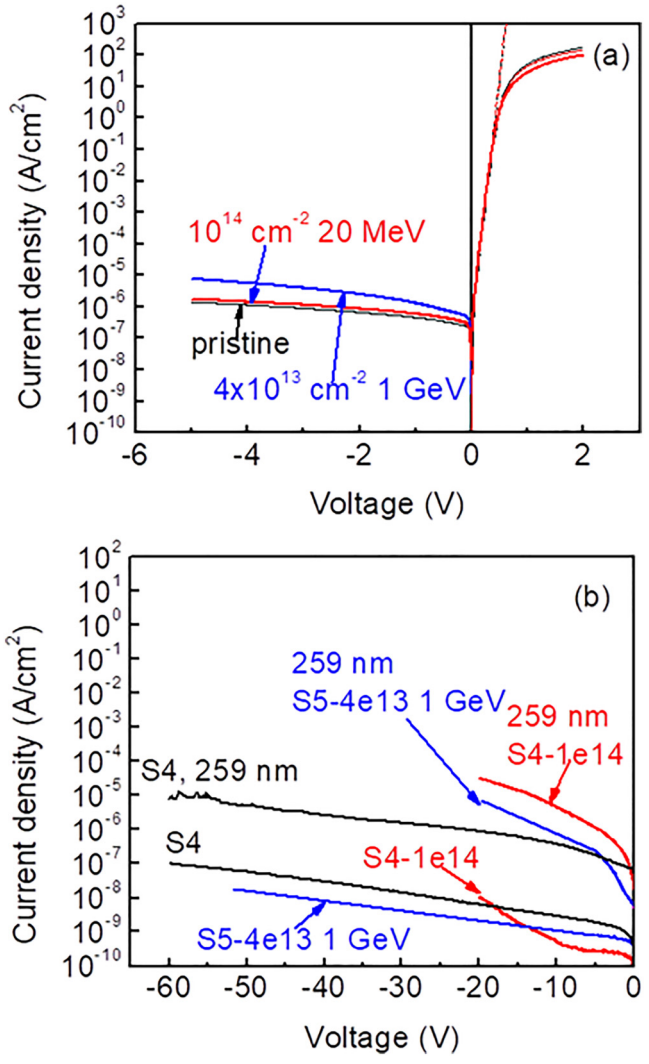

FIG. 7. (a) I-V changes induced for samples 6 and 7 by proton irradiations with 20 MeV and 1 GeV; (b) changes in the reverse current of samples S4 and S5 in the dark and under illumination with 259 nm wavelength LED as a result of proton irradiation with energy 20 MeV and 1 GeV.

It was interesting to compare the effects of proton irradiation on I-V characteristics. The results are summarized in Figs. 7(a) and 7(b). For the samples with W Schottky diodes, the effect mainly consisted of an increase in reverse current and series resistance. Figure 7(a) shows the changes induced by 10^{14} cm^{-2} 20 MeV protons in the low voltage current density of sample S6 and by 4×10^{13} cm^{-2} 1 GeV protons for sample S7 (for both samples with W Schottky diodes, the starting I-V characteristics were similar). The 20 MeV proton irradiation increased the reverse current by about two times, while the 1 GeV irradiation increased the current by about six times, while respective series resistances increased from 4.8to 6.2 Ω (1 GeV) and to 49 Ω (20 MeV). At −50 V, the reverse current after 20 MeV 10^{14} cm^{-2} irradiation increased from 5×10^{-5} to 7.5×10^{-5} A/cm^2, while the 4×10^{13} cm^{-2} 1 GeV irradiation increased the reverse current to 4×10^{-4} A/cm^2.

For sample S4, 20 MeV proton irradiation with a fluence of 10^{14} cm^{-2} depleted the film almost to the n$^+$ substrate [Fig. 2(a)]. As a result, the current at low voltages became considerably lower than before irradiation, but once the space charge region boundary passed the n-Ga_2O_3(film)/ n$^+$$Ga_2O_3$ (substrate) interface, the current grew rapidly [Fig. 7(b)]. Irradiation with 4×10^{13} cm^{-2} 1 GeV protons led to a more moderate decrease in the net donor concentration [Fig. 2(a)] and, consequently, to only a moderate decrease in reverse current density by about three times and no change in reverse current slope for voltages up to −50 V [Fig. 7(b)]. The series resistance increased after 1 GeV protons irradiation from 10.8to 17.7 Ω because of the reduced net donor density. With the 20 MeV proton irradiation, we observed that even moderate heating during DLTS runs could significantly change the net donor density. It was readily converted into respective changes of the series resistance that was very high right after irradiation (2.6×10^5 Ω), but after the first DLTS, run decreased to 430Ω, and after the second DLTS, run decreased to 24 Ω (see Fig. 6S in the supplementary material).

We have also seen that, for the S4 and S5 samples, proton irradiation significantly increased the density of deep compensating acceptors in the lower half of the bandgap, stronger for 20 MeV protons (Table I). Hole trapping on these deep acceptors is instrumental in increasing the photocurrent of the diodes under above-bandgap illumination because of the decrease in the Schottky barrier height and respective photocurrent amplification.[42,43] We observed that proton irradiation strongly enhances photocurrent, considerably stronger for 20 MeV protons creating a higher density of deep acceptors than the 1 GeV protons [Fig. 7(b)].

One can note that the behavior of reverse voltage with proton irradiation is different for samples with Ni Schottky diodes and samples S6 and S7 with W Schottky diodes. For the former, the reverse current decreased after irradiation until the space charge region in the film extended down to the film/substrate interface. For the latter, the reverse current increased with irradiation, considerably faster for the 1 GeV protons. Possible reasons for such differences in behavior are under study.

Finally, the changes induced by proton irradiation in the diffusion lengths of nonequilibrium charge carriers were estimated by EBIC. These were performed for sample S4 before and after irradiation with 10^{14} cm^{-2} 20 MeV protons, for sample S5 before and after irradiation with 4×10^{13} cm^{-2} 1 GeV protons, for sample S6 before and after irradiation with 10^{14} cm^{-2} 20 MeV protons, and for sample S7 before and after irradiation with 4×10^{13} cm^{-2} 1 GeV protons. For all starting samples, the diffusion length was close to 0.2 μm and decreased to 0.1–0.12 μm after irradiation due to the increase in the concentration of deep electron traps. The effects of 20 MeV and 1 GeV proton irradiations were not radically different.

IV. CONCLUSIONS

Proton irradiation at 1 GeV and 20 MeV of n-type β-Ga_2O_3(Si) films grown on n^+-Ga_2O_3 substrates leads to carrier removal rate between ~400 and ~100 cm^{-1}, higher for starting donor densities 3×10^{16} cm^{-3} than for donor densities below ~10^{16} cm^{-3} and comparable for both proton energies, in contrast to SRIM modeling predicting primary defects introduction rates to be more than two orders of magnitude higher for the 20 MeV protons. The overall concentrations of deep electron and hole traps fall far short of the densities required to account for observed carrier removal rates if they are due to compensation. This suggests the formation of neutral complexes between shallow donors and native point defects produced by irradiation as a cause of carrier removal. The formation of the complexes proceeds more efficiently closer to the surface.

The results of C-V profiling carried out after irradiation and after high-temperature treatments indicate that defects rearrangements begin at ~400 K and are enhanced in the presence of high electric fields. The nature of defects responsible for donor "passivation" needs further study. The participation of hydrogen in the process seems to be unlikely because of the very low density of primary hydrogen atoms introduced by protons[44] and the necessity of relatively high temperatures ~500 °C for the onset of hydrogen diffusion in β-Ga_2O_3.[30,31] For some of the native defects in Ga_2O_3 known to be deep acceptors, the defect movement at room temperature has been reported.[36] More effective carrier removal in the case of 1 GeV protons when taking into account the number of primary native defects could be a consequence of a lower rate of recombination of primary defects for higher starting energy of recoil atoms and possibly the enhanced radiation diffusion rate of defects in the presence of high densities of electrons and holes created by protons imparting their energy to the lattice.

The changes induced in reverse currents of irradiated diodes depend on the type of Schottky diodes used. For W Schottky diodes, the reverse current increases with irradiation and the increase is more pronounced for GeV irradiation. With Ni Schottky diodes, the reverse currents tend to decrease with irradiation, but, for strong radiation changes of donor density, the reverse current at high reverse voltages can increase when the space charge region extends beyond the entire thickness of the film. The series resistance of heavily irradiated films gradually increases with the decrease in donor density. For heavily compensated films in which the space charge region extends to the full width of the film, the series resistance can become very high and show a strong decrease after high-temperature treatments. The 1 GeV irradiation is more benign because of the lower carrier removal rate. More understanding could be obtained by measurements performed for a wider range of donor densities, irradiations performed at low temperatures, and for samples irradiated without the Schottky diodes already deposited.

SUPPLEMENTARY MATERIAL

See the supplementary material for additional electrical characterization results for the proton-irradiated material to support the main conclusions in this paper.

ACKNOWLEDGMENTS

The work at NUST MISiS was supported in part by the Russian Science Foundation, Grant No. 19-19-00409. The work at UF was sponsored by Department of the Defense, Defense Threat Reduction Agency, Interaction of Ionizing Radiation with Matter University Research Alliance (Award No. HDTRA1-20-2-0002) monitored by J. Calkins and also by the National Science Foundation (NSF) under No. DMR 1856662 (James Edgar).

AUTHOR DECLARATIONS

Conflict of Interest

The authors have no conflicts to disclose.

DATA AVAILABILITY

The data that support the findings of this study are available within the article.

REFERENCES

[1]S. J. Pearton, J. Yang, P. H. Cary, IV, F. Ren, J. Kim, M. J. Tadjer, and M. A. Mastro, Appl. Phys. Rev. **5**, 011301 (2018).
[2]S. J. Pearton, F. Ren, M. Tadjer, and J. Kim, J. Appl. Phys. **124**, 220901 (2018).
[3]J. Zhang, J. Shi, D.-C. Qi, L. Chen, and K. H. L. Zhang, APL Mater. **8**, 020906 (2020).
[4]M. Higashiwaki and S. Fujita, *Gallium Oxide Materials Properties, Crystal Growth, and Devices* (Springer, Switzerland, 2020).
[5]J. Kim, S. J. Pearton, C. Fares, J. Yang, F. Ren, S. Kim, and A. Y. Polyakov, J. Mater. Chem. C **7**, 10 (2018).
[6]S. J. Pearton, F. Ren, J. Kim, M. Stavola, and A. Y. Polyakov, "Radiation damage in Ga_2O_3 materials and devices," in *Wide Bandgap Semiconductor-Based Electronics*, edited by F. Ren and S. J. Pearton (IOP Publishing, Bristol, 2020). Chap. 7.
[7]S. J. Pearton, A. Aitkaliyeva, M. Xian, F. Ren, A. Khachatrian, A. Ildefonso, Z. Islam, M. A. Jafar Rasel, A. Haque, A. Y. Polyakov, and J. Kim, ECS J. Solid State Sci. Technol. **10**, 055008 (2021).
[8]A. Y. Polyakov, N. B. Smirnov, I. V. Shchemerov, E. B. Yakimov, J. Yang, F. Ren, G. Yang, J. Kim, A. Kuramata, and S. J. Pearton, Appl. Phys. Lett. **112**, 032107 (2018).
[9]M. E. Ingebrigtsen, A. Y. Kuznetsov, B. G. Svensson, G. Alfieri, A. Mihaila, U. Badstübner, A. Perron, L. Vines, and J. B. Varley, APL Mater. **7**, 022510 (2019).
[10]E. Farzana, M. F. Chaiken, T. E. Blue, A. R. Arehart, and S. A. Ringel, APL Mater. **7**, 022502 (2019).
[11]A. Y. Polyakov, N. B. Smirnov, I. V. Shchemerov, A. A. Vasilev, E. B. Yakimov, A. V. Chernykh, A. I. Kochkova, P. B. Lagov, Y. S. Pavlov, O. F. Kukharchuk,

A. A. Suvorov, N. S. Garanin, I.-H. Lee, M. Xian, F. Ren, and S. J. Pearton, J. Phys. D: Appl. Phys. **53**, 274001 (2020).
[12]A. Y. Polyakov, N. B. Smirnov, I. V. Shchemerov, E. B. Yakimov, S. J. Pearton, C. Fares, J. Yang, F. Ren, J. Kim, P. B. Lagov, V. S. Stolbunov, and A. Kochkova, Appl. Phys. Lett. **113**, 092102 (2018).
[13]Z. Zhang, E. Farzana, A. R. Arehart, and S. A. Ringel, Appl. Phys. Lett. **108**, 052105 (2016).
[14]E. Farzana, E. Ahmadi, J. S. Speck, A. R. Arehart, and S. A. Ringel, J. Appl. Phys. **123**, 161410 (2018).
[15]J. V. Li and G. Ferrari, *Capacitance Spectroscopy of Semiconductors* (Pan Stanford Publishing Pte Ltd, Singapore, 2018), p. 437.
[16]A. Y. Polyakov, N. B. Smirnov, I.-H. Lee, and S. J. Pearton, J. Vac. Sci. Technol. B **33**, 061203 (2015).
[17]A. Blondeel, P. Clauws, and D. Vyncke, J. Appl. Phys. **81**, 6767 (1997).
[18]A. Y. Polyakov, N. B. Smirnov, I. V. Shchemerov, S. J. Pearton, F. Ren, A. V. Chernykh, P. B. Lagov, and T. V. Kulevoy, APL Mater. **6**, 096102 (2018).
[19]A. Y. Polyakov, I.-H. Lee, N. B. Smirnov, I. V. Shchemerov, A. A. Vasilev, A. V. Chernykh, and S. J. Pearton, J. Phys. D: Appl. Phys. **53**, 304001 (2020).
[20]E. B. Yakimov, A. Y. Polyakov, N. B. Smirnov, I. V. Shchemerov, J. Yang, F. Ren, G. Yang, J. Kim, and S. J. Pearton, J. Appl. Phys. **123**, 185704 (2018).
[21]E. B. Yakimov, A. Y. Polyakov, N. B. Smirnov, I. V. Shchemerov, P. S. Vergeles, E. E. Yakimov, A. V. Chernykh, M. Xian, F. Ren, and S. J. Pearton, J. Phys. D: Appl. Phys. **53**, 495108 (2020).
[22]P. B. Lagov, A. S. Drenin, and M. A. Zinoviev, J. Phys.: Conf. Ser. **830**, 012152 (2017).
[23]Y. S. Pavlov, A. M. Surma, P. B. Lagov, Y. L. Fomenko, and E. M. Geifman, J. Phys.: Conf. Ser. **747**(1), 012085 (2016).
[24]N. K. Abrossimov, E. M. Ivanov, Y. T. Mironov, G. A. Riabov, and M. G. Tverskoy, "Proton beam of variable energy—The new tool for investigation of radiation effects at PNPI synchrocyclotron," in *IEEE Radiation Effects Data Workshop*, *2003 January* (IEEE, 2003), pp. 145–148.
[25]E. M. Ivanov, O. A. Shcherbakov, A. S. Vorobyev, A. M. Gagarski, V. S. Anashin, S. A. Artamonov, G. F. Mikheev, and S. Oberstedt, EPJ Web Conf. **146**, 03009 (2017).
[26]S. A. Artamonov, E. M. Ivanov, N. A. Ivanov, J. S. Lebedeva, and G. A. Riabov, Phys. Part. Nucl. Lett. **14**, 188 (2017).
[27]See http://www.srim.org/ for the tutorial and software download site.
[28]J. F. Ziegler, M. D. Ziegler, and J. P. Biersack, Nucl. Instrum. Methods Phys. Res. Sect. B **268**, 1818 (2010).
[29]D. K. Schroder, *Semiconductor Material and Device Characterization* (Wiley & Sons, Inc., New York, 1990), Chap. 7.
[30]V. M. Reinertsen, P. M. Weiser, Y. K. Frodason, M. E. Bathen, L. Vines, and K. M. Johansen, Appl. Phys. Lett. **117**, 232106 (2020).
[31]A. Karjalainen, P. M. Weiser, I. Makkonen, V. M. Reinertsen, L. Vines, and F. Tuomisto, J. Appl. Phys. **129**, 165702 (2021).
[32]A. Karjalainen, V. Prozheeva, K. Simula, I. Makkonen, V. Callewaert, J. B. Varley, and F. Tuomisto, Phys. Rev. B **102**, 195207 (2020).
[33]J. B. Varley, H. Peelaers, A. Janotti, and C. G. Van de Walle, J. Phys.: Condens. Matter **23**, 334212 (2011).
[34]P. Deák, Q. D. Ho, F. Seemann, B. Aradi, M. Lorke, and T. Frauenheim, Phys. Rev. B **95**, 075208 (2017).
[35]M. E. Ingebrigtsen, J. B. Varley, A. Y. Kuznetsov, B. G. Svensson, G. Alfieri, A. Mihaila, U. Badstübner, and L. Vines, Appl. Phys. Lett. **112**, 042104 (2018).
[36]Y. K. Frodason, C. Zimmermann, E. F. Verhoeven, P. M. Weiser, L. Vines, and J. B. Varley, Phys. Rev. Mater. **5**, 025402 (2021).
[37]A. T. Neal, S. Mou, S. Rafique, H. Zhao, E. Ahmadi, J. S. Speck, K. T. Stevens, J. D. Blevins, D. B. Thomson, N. Moser, K. D. Chabak, and G. H. Jessen, Appl. Phys. Lett. **113**, 062101 (2018).
[38]A. Y. Polyakov, N. B. Smirnov, I. V. Shchemerov, S. J. Pearton, F. Ren, A. V. Chernykh, and A. I. Kochkova, Appl. Phys. Lett. **113**, 142102 (2018).
[39]C. Zimmermann, E. Førdestrøm Verhoeven, Y. Kalmann Frodason, P. M. Weiser, J. B. Varley, and L. Vines, J. Phys. D **53**, 464001 (2020).
[40]E. B. Yakimov and A. Y. Polyakov, "Defects and carrier lifetimes in Ga_2O_3," in *Wide Bandgap Semiconductor-Based Electronics*, edited by F. Ren and S. J. Pearton (IOP Publishing, Bristol, 2020), Chap. 5.
[41]H. Peelaers, J. L. Lyons, J. B. Varley, and C. G. Van de Walle, APL Mater. **7**, 022519 (2019).
[42]E. B. Yakimov, A. Y. Polyakov, I. V. Shchemerov, N. B. Smirnov, A. A. Vasilev, P. S. Vergeles, E. E. Yakimov, A. V. Chernykh, A. S. Shikoh, F. Ren, and S. J. Pearton, APL Mater. **8**, 111105 (2020).
[43]E. B. Yakimov, A. Y. Polyakov, I. V. Shchemerov, N. B. Smirnov, A. A. Vasilev, A. I. Kochkova, P. S. Vergeles, E. E. Yakimov, A. V. Chernykh, M. Xian, F. Ren, and S. J. Pearton, J. Alloys Compd. **879**, 160394 (2021).
[44]A. Venzie, A. Portoff, C. Fares, M. Stavola, W. Beall Fowler, F. Ren, and S. J. Pearton, Appl. Phys. Lett. **119**, 062109 (2021).